Journal of Structural Geology 32 (2010) 1147–1157

Contents lists available at ScienceDirect

Journal of Structural Geology

journal homepage: www.elsevier.com/locate/jsg

Rotation of irregular staurolite porphyroblasts in a simple shear dominated shear zone controlled by initial growth orientation and aspect ratio

Jochen E. Mezger*

Institut für Geowissenschaften, Martin-Luther-Universität Halle-Wittenberg, 06120 Halle, Germany

ARTICLE INFO

Article history:
Received 17 January 2010
Received in revised form
25 June 2010
Accepted 4 July 2010
Available online 14 July 2010

Keywords:
Staurolite porphyroblasts
Porphyroblast rotation
Best-fit ellipse
Shear strain
Shear zone

ABSTRACT

In a mica schist unit of the Bossòst dome (Central Pyrenees, Spain) idioblastic interkinematic staurolite porphyroblasts with straight inclusion trails (S_i) have rotated with respect to the main schistosity in the same sense by different amounts. Orientation data of 600 porphyroblasts were obtained from planes parallel to stretching lineation (xz), perpendicular to lineation (yz) and parallel to schistosity (xy). Interpenetrating growth twinning resulted in highly irregular shapes with aspect ratios (R_A) ranging from 1 to 5. Initial random porphyroblast growth is inferred from variable length axis (LA)–S_i angles. Maximum rotation of 120° is observed in blasts with S_i oriented orthogonal to the mineral long axis, implying a shear strain of $\gamma = 4.3$ in simple shear flow. Absence of back rotation is indicative of dominant simple shear flow ($W_K \geq 0.8$–0.9). Elongated porphyroblasts ($R_A > 3$) with S_i parallel to LA have rotated very little, because they were already in a stable position when shearing commenced. Rotation of staurolite porphyroblasts was possible because decoupling between blasts and matrix was weak and no significant strain partitioning had developed. The wide variety of shapes with different aspect ratios formed by simple blasts and interpenetrating growth twins of staurolite are potential shear strain and vorticity gauges.

1. Introduction

The kinematic behaviour of porphyroblasts has been the focus of interest for anyone working in metamorphic terranes, ever since Zwart (1962) recognized the interaction of porphyroblast growth and deformation. While the discussion about whether rigid porphyroblasts in deforming ductile rocks can rotate at all or not with respect to an external reference frame is still ongoing (Bons et al., 2009; Fay et al., 2008; Lister and Forster, 2009), the majority of research published acknowledges the possibility of porphyroblast rotation (e.g. Robyr et al., 2009 for a recent study). Minerals whose kinematic behaviours are studied include garnet (Robyr et al., 2009; Schoneveld, 1977; Williams and Jiang, 1999), staurolite (Busa and Gray, 1992; Johnson et al., 2006; Mezger and Passchier, 2003), biotite (Holcombe and Little, 2001; Miyake, 1993), and plagioclase (Johnson, 2009). Linking ductile deformation to metamorphism allows distinction of individual tectonic and metamorphic events and establishment of their relative chronological order (Mezger and Passchier, 2003). Under certain conditions, strain rates and vorticity numbers can be deduced from rotated porphyroblasts (Biermeier and Stüwe, 2003; Holcombe and Little, 2001; Johnson et al., 2009).

A characteristic mineral of amphibolite facies regional metamorphism is staurolite, commonly forming euhedral poikiloblastic porphyroblasts, which can contain inclusion trails that preserve earlier fabrics. In contrast to the equant habit of garnets, staurolite porphyroblasts possess elongated prismatic shapes of various aspect ratios, often forming a variety of interpenetrating growth twins, such as crosses (Ribbe, 1982). The stability field of staurolite is also restricted roughly to medium pressure–medium temperature conditions commonly associated with regional metamorphism resulting from crustal thickening during earlier orogenic stages. Widespread magmatism occurs in later phases of the development of many orogens, evident from late-tectonic pluton emplacement. As a consequence, contact metamorphism around the intrusions overprints previously regionally metamorphosed rocks. Newly formed porphyroblasts within the contact aureole, such as andalusite and cordierite, grow at the expense of earlier phases (e.g. staurolite), which suffer resorption along grain boundaries, leading to loss of euhedral shape, possible reduction to relics within the new overgrowing phases, and ultimately to complete absorption (Mezger et al., 2001; Mezger and Passchier, 2003). Interpretation of flow behaviour and deduction of sense of shear from partially consumed phases, having lost their original shape, become difficult (Mezger, 2010).

* Fax: +49 (0) 345 5527220.
E-mail address: jochen.mezger@geo.uni-halle.de.
URL: http://www.elsevier.com/researchhighlights

0191-8141/$ – see front matter © 2010 Elsevier Ltd. All rights reserved.
doi:10.1016/j.jsg.2010.07.002

Despite these limitations, idioblastic staurolite crystals in rocks having undergone ductile non-coaxial flow can be observed under specific circumstances. In a shear zone within the Bossòst dome of the Central Pyrenees, Spain, favourable whole rock chemistry preserves staurolite in mica schist layers, while in adjacent rocks it is being replaced by andalusite and cordierite associated with younger contact metamorphism (Mezger and Passchier, 2003; Mezger et al., 2004; Mezger, 2010). In the direction of shear, staurolite porphyroblasts with high aspect ratios tend to lie with their long axis parallel to the schistosity plane. Straight inclusion trails oriented at various angles with the external foliation led Mezger and Passchier (2003) to conclude that staurolite crystals rotated, with respect to the main schistosity, in the same sense by different amounts until a stable position parallel to the shear plane was attained. These observations are in accordance with results from analogue and numerical models that show elongated rigid objects become stationary during general flow (Marques and Coelho, 2003; Passchier, 1987; Passchier and Trouw, 2005; ten Grotenhuis et al., 2002) or simple shear (Arbaret et al., 2001; Mancktelow et al., 2002; Marques and Coelho, 2001). Various angles of the internal foliation (S_i), represented by straight quartz inclusion trails, with the external foliation (S_e) indicate that rotation of staurolite porphyroblasts was not uniform and depended on their aspect ratios and their orientation in space with respect to the kinematic frame of the bulk flow prior to the onset of deformation (Holcombe and Little, 2001; Johnson, 2009).

To test the conclusions of Mezger and Passchier (2003), which were based on a small number of staurolite porphyroblasts, statistical analyses of a larger data pool were carried out. In this study the aspect ratios and angular relations of crystal long axes and inclusion trails with external schistosity were determined on 628 staurolite porphyroblasts from the Bossòst sample locality in sections parallel to mineral lineation and perpendicular to schistosity (xz), orthogonal to mineral lineation and schistosity (xy) and parallel to the schistosity plane (xy). In addition, the obtained aspect ratios and amount of rotation allows estimation of finite strain and vorticity. The results show that porphyroblasts in a simple shear dominated flow can rotate relative to one another. The amount of rotation is controlled largely by initial orientation of the crystal prior to onset of shearing and its shape, i.e. aspect ratio, of the porphyroblast, which varies significantly among staurolite grains. This implies a strong coupling between blast and matrix, and weak strain partitioning around the staurolite porphyroblasts, which originates from the particular lithology of the schist unit. The rheological properties of this staurolite schist are different to those required for the porphyroblast non-rotation model of Bell (1985).

2. Geological setting

The examined sample is a staurolite–mica schist from the Bossòst structural–metamorphic dome of the Axial Zone in the Spanish Central Pyrenees (Fig. 1). The dome is an elongated, 30 km long, roughly E–W-trending structure, formed during the main Variscan deformation phase by the intrusion of Carboniferous leucogranites into Cambro–Ordovician metasedimentary rocks. Granite emplacement was facilitated by NW–SE-directed extension (D_{2a}) along a flat-lying shear zone which developed during local strain partitioning in an overall N–S compressive setting (Mezger and Passchier, 2003). Continuous granite emplacement (D_{2a}) and subsequent SSW–NNE compression (D_3) led to the formation of domal shaped doubly plunging antiforms. Southward thrusting of the northern block along the E–W-trending Bossòst fault created the present structural constellation: a northern half-dome with an exposed granitic core, and a southern doubly plunging antiform.

Two metamorphic phases can be distinguished: an early medium pressure–medium temperature regional metamorphism (5.5 kbar, 580 °C), recorded in garnet–staurolite schist, and a later high-temperature contact metamorphism, preserved in sillimanite–cordierite–biotite assemblages, locally migmatized, related to the intrusion of the Carboniferous Bossòst granite (Mezger et al., 2004). Inclusion trails in staurolite porphyroblasts are straight. In some blasts S_i can be traced into the external schistosity, implying static intertectonic growth postdating formation of the main S_1 schistosity. Within an approximately 1.5 km thick shear zone in the eastern southern antiform, staurolite inclusion trails oblique to S_e indicate uniform top-to-the-SE shearing during D_{2a}. Andalusite and cordierite in the contact aureole grew syntectonically under coaxial conditions (D_{2b}), while older staurolite grains are anhedral or occur as relics within cordierite.

3. Sample description

A narrow layer of staurolite–mica schist crops out at the eastern end of the southern Bossòst antiform, 500 m northwest of the village of Arres on the northern slope of the Val d'Aran. At this locality (0°42′24″ E, 42°46′15″ N), a staurolite schist unit structurally overlies cordierite schist at the top of an SE-directed shear zone separating amphibolite facies Cambro–Ordovician metasedimentary rocks from overlying upper Ordovician marble and Silurian black slate. The moderately southward dipping schist unit forms the southern limb of the antiform. A prominent mineral lineation plunges shallowly to the east-southeast. Oriented subparallel to the lineation a millimeter-scale crenulation fold axes can be observed. In other areas of the southern Bossòst dome, this crenulation folds the lineation, indicating that these fabrics were not developed simultaneously (Mezger and Passchier, 2003).

The garnet-bearing staurolite–mica–quartz schist possesses a well-developed spaced schistosity. Cleavage domains are composed of fine-grained (<300 μm) aligned biotite and muscovite and account for approximately 50% of the rock volume. The mica-rich zones vary in thickness from 1 to 3 mm and their transition with microlithons can be discrete or gradational. Fine-grained quartz (50–200 μm) and interspersed aligned biotite produce a continuous schistosity within the microlithons. The appearance of the foliation is most likely the result of a combination of transposed pelitic and psammatic beds and tectonic activity, i.e. formation of schistosity.

Staurolite is abundant (5–15 vol.%) and forms large (≤1 cm) idioblastic porphyroblasts with straight crystal faces. Interpenetrating growth twinning with a variety of shapes is developed in the majority of the staurolite porphyroblasts (Fig. 2a, c). Staurolite overgrew mica- and quartz-rich domains, preserved as inclusion-poor and inclusion-rich zones, which gives porphyroblasts a striped appearance in polished sections. Biotite porphyroblasts, up to 1 mm size, are truncated by the biotite–muscovite schistosity. Rare almandine garnets can measure up to 2 mm in diameter. While staurolite crystals in the sample discussed here show no signs of corrosion or recrystallization, in the nearby cordierite schist unit, staurolite suffers resorption and is partially overgrown by andalusite and cordierite, which were formed by staurolite-consuming reactions (Mezger and Passchier, 2003). A deficiency in MgO in the studied rock has prevented growth of cordierite, thus preserving staurolite under metastable conditions (Mezger et al., 2004).

In sections parallel to the lineation (xz), inclusion trails (S_i) are straight. In some porphyroblasts, S_i continues directly into the external foliation (S_e), indicating that staurolite statically overgrew an existing schistosity (Fig. 2a, b). Varying obliquity of S_i to S_e with the same sense suggests rotation by various degrees in the same direction. A small number of twinned porphyroblasts appear to have been broken or fractured, but no signs of dynamic recrystallization or plastic deformation of staurolite crystals are observed.

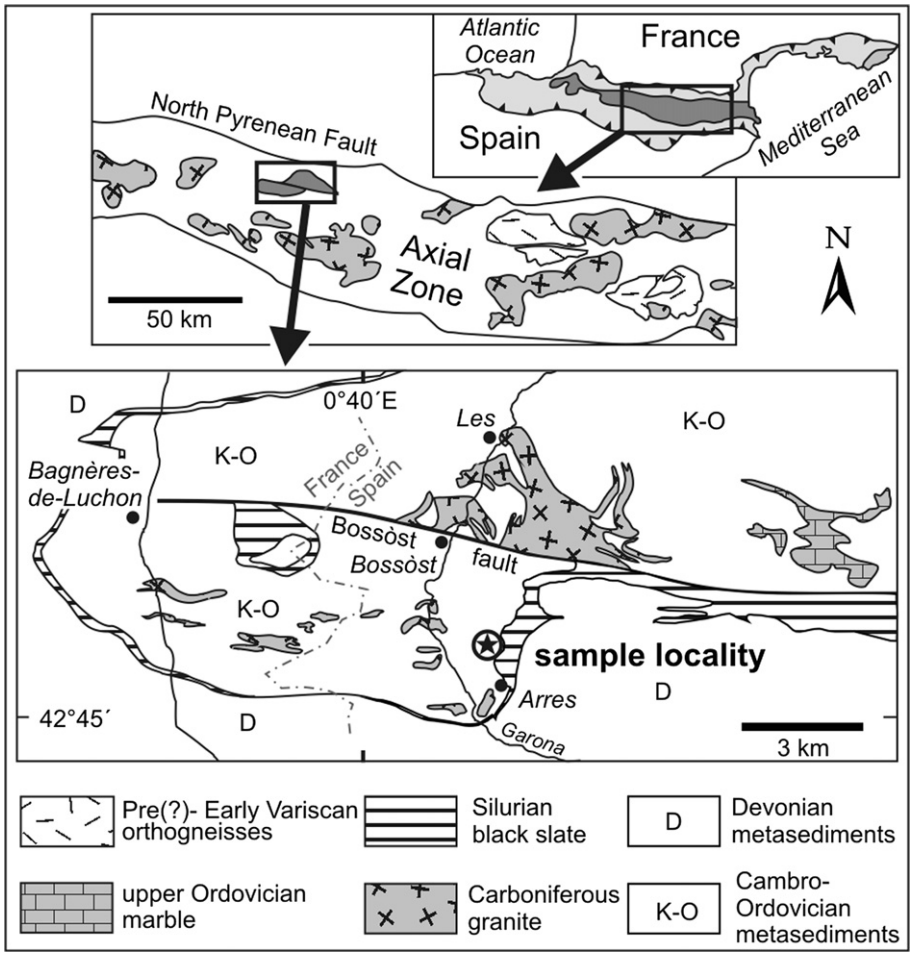

Fig. 1. Geological overview map of the Bossòst dome with sample locality. Modified after de Sitter and Zwart (1960) and Mezger et al. (2004).

Biotite mica fishes show the same sense of shear as the rotated staurolite grains. Quartz inclusions in staurolite are generally smaller than matrix quartz grains and possess elongated rounded shapes. This may indicate coarsening of matrix quartz by dynamic recrystallization after formation of staurolite. Sections perpendicular to lineation (yz) show that crenulation folds S_e, but not S_i, therefore crenulation folds postdate staurolite growth. In the yz-plane, a larger percentage of staurolite grains (40%), predominantly smaller ones which do not incorporate contact between mica- and quartz-rich layers, do not possess discernable S_i and their quartz inclusions have equant shapes.

4. Methodology

Sample material was collected across a few metres within the staurolite schist layer. From thin sections made in xz- and yz-planes the following parameters were obtained: 1) length of long axis, 2) aspect ratio R_A of long and short axes, 3) angle α between long axis and S_e, 4) angle β between S_i and S_e, 5) angle λ between long axis and S_i, and 6) the ratio L^* between lengths of long axis and S_i (Fig. 3). Parallel to schistosity (xy) samples were cut, polished and scanned, and in addition to R_A, the angles between mineral lineation and long axis (δ) and lineation and S_i (ε) were measured.

Of those parameters, only β and ε are determined directly from thin section or sample scan, while the others are controlled by the shape and orientation of the blast. The variety of shapes, especially of twinned staurolites, does not allow simple determination of long axes and aspect ratios by visual approximation. To solve this problem, best-fit ellipses for each porphyroblast were determined with the software ImageJ[1] using the following routine. The thin section or polished rock face is scanned and enlarged. The shapes of the porphyroblasts are traced and a uniform colour fill is assigned to enhance the poor contrast difference of the original scans. ImageJ calculates long and short axes of the best-fit ellipses and the angle α, provided that S_e in the image is aligned to the horizontal. A separate bitmap with the ellipses is also created (Fig. 2). L^* is determined by the calculated length of the long axis and by measuring the length of S_i within the ellipse, passing through the centre of the ellipse at the observed angle β (Fig. 3).

The size of the porphyroblasts at this location, at maximum 1 cm, is not sufficient enough to produce serial sections – at least at the laboratory facilities available to the author – that would allow a three-dimensional reconstruction of individual blasts. Thus, each section is only a two-dimensional representation of a possibly more complex shape. In addition, each section reveals cross sections that randomly cut porphyroblasts, not necessarily through the centre of the grain, so that its shape may change considerably in parts of the slab that are orthogonal to the section and that are destroyed in the thin section-making process. Therefore, length and aspect ratios

[1] ImageJ is a Windows-based analysis software from the National Institute of Health (NIH), available at http://rsbweb.nih.gov/ij/index.html (last accessed June 18, 2010), originally programmed for Mackintosh computers under name NIH Image, as used by Mancktelow et al. (2002).

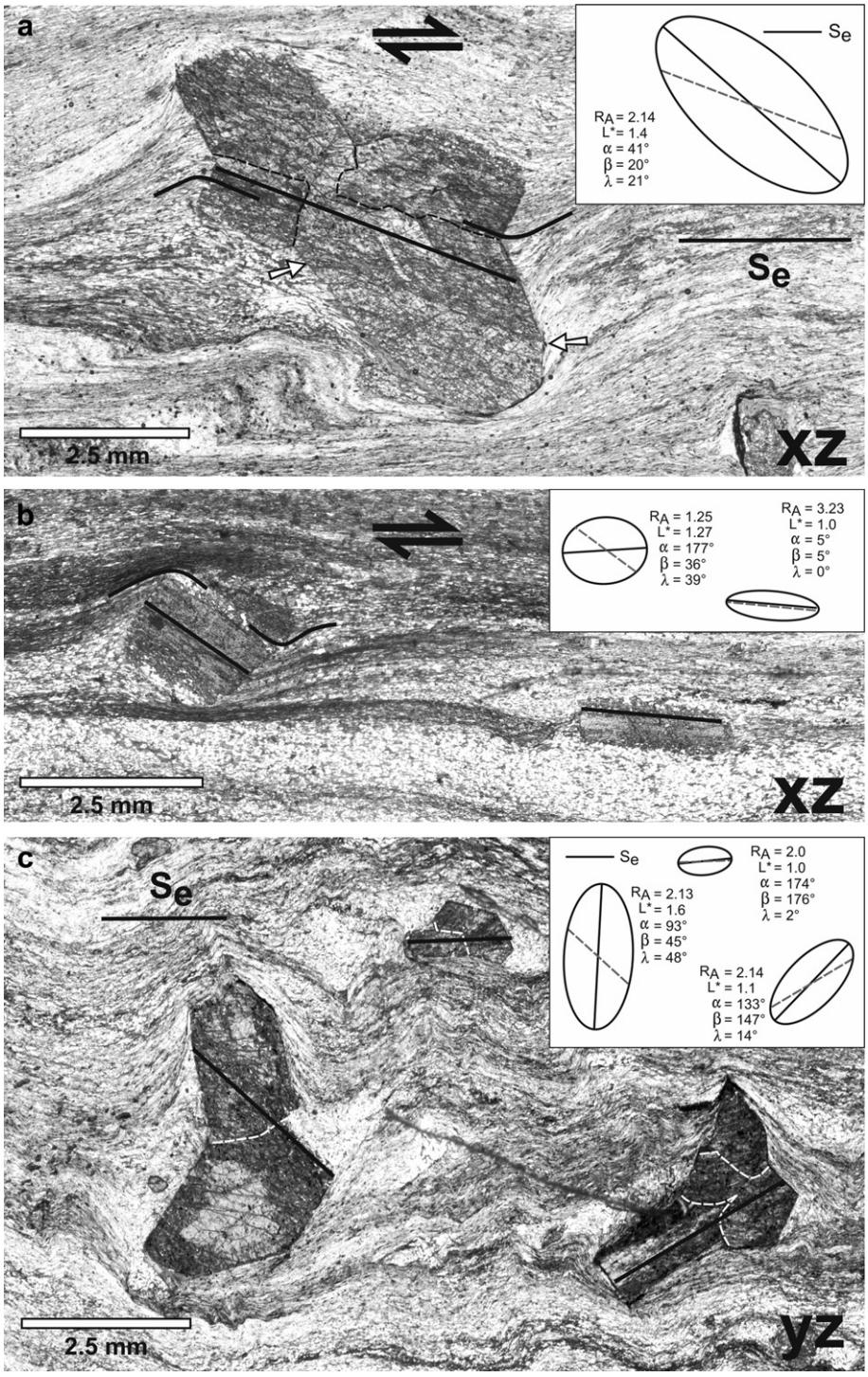

Fig. 2. Thin section scans of staurolite schist and best-fit ellipse analyses of staurolite porphyroblasts calculated by the freeware ImageJ. Idioblastic, irregularly shaped staurolite porphyroblasts in a fine-grained matrix of muscovite + biotite + quartz + illmenite+graphite possess internal foliation S_i (thick black line in scan, dashed grey line in ellipse), easily recognized by contrast of inclusion-rich and -poor zones (white arrows) where the blast overgrew mica- and quartz-rich layers, respectively. Boundaries of interpenetrating growth twins within staurolite are indicated by dashed lines. (a) Section (xz) parallel stretching lineation. Drag symmetry of S_e near grain boundary indicates clockwise rotation, a dextral sense of shear, confirmed by biotite fish in the matrix. The long axis of the blast (black line in ellipse) originally lay at small angles antithetically to the later flow direction, and subsequently rotated synthetically by 20°. (b) Section parallel to the mineral lineation. The long axes of two staurolite porphyroblasts with significantly different aspect ratios lie parallel to the shear plane. The amount of rotation is given the angle β (S_i–S_e). While the more equant left blast ($R_A = 1.25$) has rotated about 39° clockwise, the elongated right blast ($R_A = 3.23$) with long axis parallel inclusion trails ($\lambda = 0°$) has rotated very little, since its long axis was already in a stable position prior to the onset of shearing. (c) Section (yz) perpendicular mineral lineation. Crenulation folding can be observed in the fine-grained matrix and is concentrated at tips of staurolite grains. Long axes are oriented either parallel to the external schistosity or close to orthogonal to it. S_i is tilted in both directions with respect to S_e, and is most likely the result of D_3 shortening which rotated the elongated staurolite twins into steeper oriented positions. R_A: ellipse aspect ratio, L^*: ratio of long axes and S_i lengths, α: angle between long axes and external foliation, β: angle between internal and external foliation, λ: angle between long axis and internal foliation.

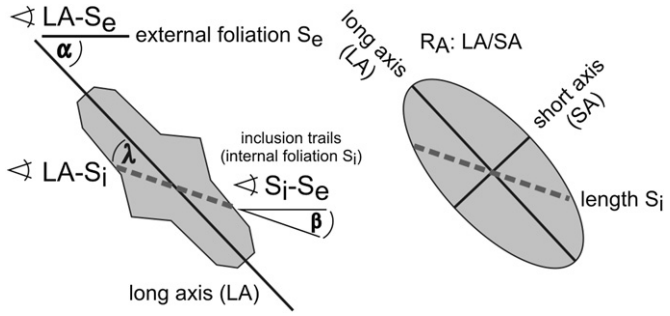

Fig. 3. Key parameters for porphyroblast characterization in the xz- and yz-planes. The angle β (S_i–S_e) can easily be measured in thin section. α and λ are dependent on the orientation of the long axis, derived from the best-fit ellipse calculated by the software ImageJ. The length of S_i is approximated by the length of a line passing through the ellipse centre. In xz-sections α and β are measured in the sense-of-shear rotation sense. The angle between the long axis and the inclusion trails (λ) ranges between 0° and 90°.

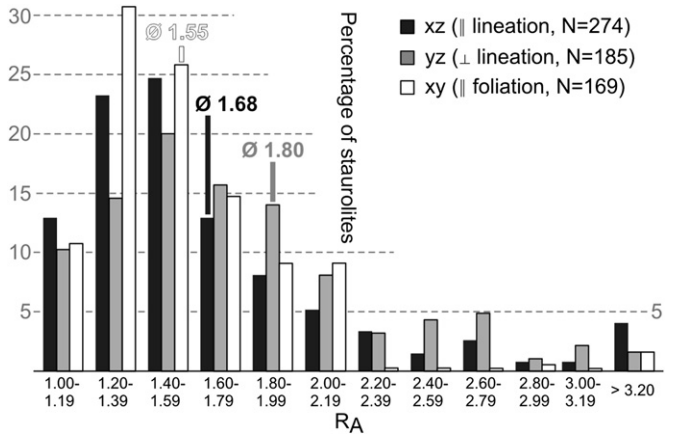

Fig. 4. Distribution diagram of staurolite porphyroblast aspect ratios (R_A) in sections parallel to lineation (xz), perpendicular to lineation (yz) and parallel to schistosity (yx). Smallest R_A is seen in the schistosity plane, higher means and higher R_A are found in the xz- and yz-planes.

refer to the random section transecting individual blasts, and do not necessarily reflect actual sizes and shapes. For the same reason, it cannot be excluded that porphyroblasts have been in contact with others and thus affect each others' flow behaviour (Tikoff and Teyssier, 1994). These inevitable uncertainties will result in some scatter of the data discussed below. Despite these limitations, microstructural observations yield conclusive results on the rotational behaviour of complex-shaped metamorphic porphyroblasts during non-coaxial deformation. In total, 274 staurolite crystals were used for analyses in xz-, 185 in yz- and 169 in xy-planes. Inclusion trails could be measured in 257 grains of the xz-, in 110 of yz- and in 102 of the xy-plane.

5. Results

5.1. Aspect ratios and angular relationships between S_e, S_i and long axes

Higher maximum aspect ratios are observed in yz-, and xz-planes, 6.1 and 5.1, respectively, than in the xy-plane (3.7). R_A in all planes form skewed bell-shaped distribution curves with a smaller mean (1.55) in xy, where R_A exceeding 2.2 are rare, compared to xz (1.68) and yz (1.80), which possess successively flatter distribution curves (Fig. 4). It follows that the staurolite schist possesses a non-random fabric.

No distinct maximum exists for the orientations of the long axes with respect to S_e, angle α, in the xz-plane (Fig. 5a). Small α values (0–30°, 140–180°) are recorded preferentially in blasts with high aspect ratios (>2). In the yz-plane, maxima are observed in high-R_A blasts at angles close to the S_e, and preferentially in low-R_A blasts nearly orthogonal to S_e ($\alpha > 70°$). Within the schistosity plane (xy), a moderate maximum, with a mean of 95° for δ, is observed at high angles to the mineral lineation.

The three orientations differ significantly in their distribution of β and ϵ angles, having distinct singular maxima. For xz a mean of 43° is observed, and some S_i display angles exceeding 90°. Low-R_A blasts tend to have larger β values than elongated staurolite grains. In yz, β values rarely exceed 50°, with a maximum at low angles (0–10°) and a mean at 20°. In xy, S_i is oriented nearly orthogonal (80–120°) to the mineral lineation, ϵ having a mean of 98°. Large β values in the xz-plane, S_i subparallel to S_e in the yz-plane and nearly perpendicular to the lineation within the schistosity plane strongly suggest that, on average, the porphyroblasts have rotated or tilted around an axis orthogonal to the shear direction, which is indicated by the mineral lineation (Fig. 5b).

5.2. Initial pre-deformational growth orientation

The presence of exclusively straight and parallel inclusion trails in staurolite porphyroblasts points to nucleation and growth after the development of the main schistosity, during a period when deformation was negligible. Consequently, staurolite crystals could have grown at random, without preferred orientation. This assumption is important for subsequent interpretations of finite staurolite orientations and the implications on the mechanical behaviour during general flow. To test this premise, the dependence of the long axis obliquity with S_e, represented by the angle α, with porphyroblast size, expressed in the length of the long axis, is examined. No correlation can be observed in the xz- and yz-planes (Fig. 6a). Likewise, porphyroblast shapes, expressed in the R_A of the best-fit ellipses, are not correlated with the angle λ between long axis and inclusion trails, neither in xz- nor in yz-plane (Fig. 6b). Variably oriented inclusion trails with respect to crystal long axes do not support a mica-rich layer controlled preferred growth direction. In conclusion, staurolite porphyroblasts of this schist unit grew in random directions during a phase of relative deformational inactivity (Fig. 6c).

5.3. Orientation after finite deformation

Mezger and Passchier (2003) have shown that the straight inclusion trails of staurolite porphyroblasts at this locality were the result of overgrowth of a parallel developed schistosity. The obliquity of S_i with S_e (β) therefore indicates the amount of apparent rotation in the respective thin section plane. The relation between rotation and long axis orientation can be examined by comparing the obliquity of the long axes with S_e (α) and S_i (λ) (Fig. 7). A small value for α and λ indicates that the blast lies subparallel with its long axis to S_i and S_e, and apparently did not rotate, or by a multitude of 180°, for which there is no further evidence. Values of 90° for α and λ imply that the blast long axis is orthogonal to S_e, while S_i parallels the external schistosity. In that case as well, the blast has not rotated. With α close to 180° and λ nearly 90°, an initially vertically oriented porphyroblast has rotated by 90°.

Fig. 8a shows that data for the xz- and yz-planes differ significantly. In the xz-plane, porphyroblasts, especially with larger R_A (>2), cluster at low-α/low-λ, implying negligible rotation, and at high-α/high-λ quadrant significant synthetic rotation. Intermediate values are scarce for high-R_A blasts. Blasts with a more equant shape (R_A 1.2–1.49) are distributed along a continuous girdle. Conspicuously

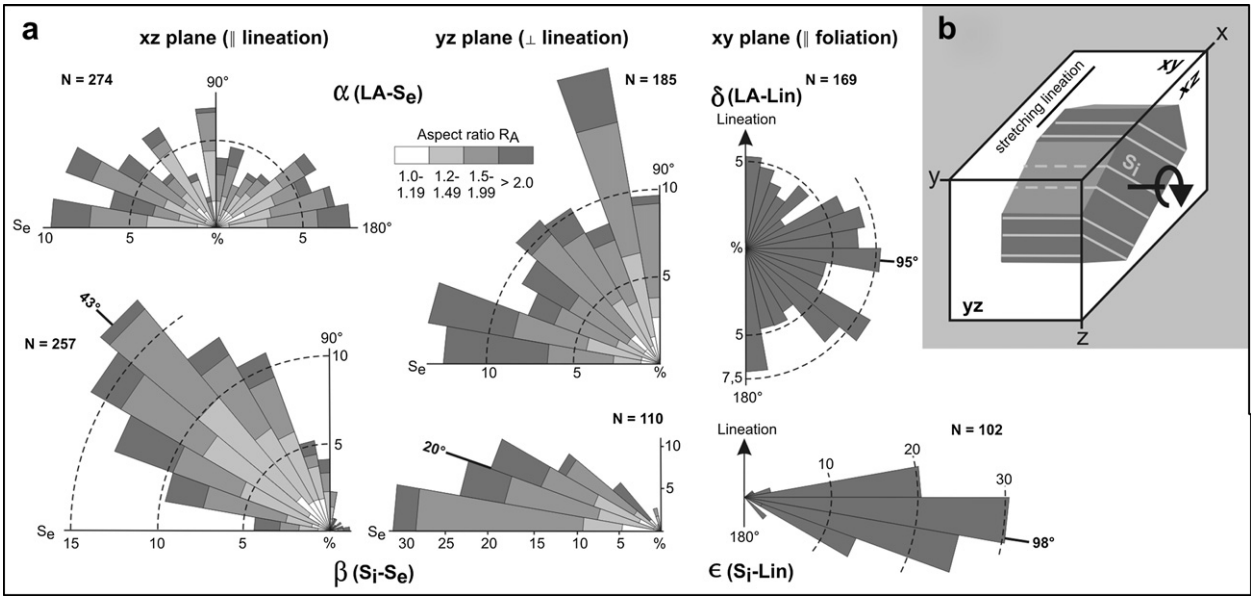

Fig. 5. (a) Rose diagrams of long axes and S_i orientations with respect to S_e in the xz- and yz-planes, and to mineral lineation in the xy-plane. Note, in the yz-plane only angles from 0 to 90° were measured, since some non-oriented thin sections were used. (b) Block diagram of an idealized porphyroblast with the mean orientations of S_i in each plane.

absent are staurolite crystals that lie in the low-α/high-λ quadrant representing antithetic rotation. High-R_A blasts do not display intermediate ($\alpha = 90°$) and small λ values, which would imply rotation of an elongated shape from an initially foliation-parallel orientation to position orthogonal to it. In the yz-plane, data distribution in the α/λ diagram is more symmetric. The main difference with the xz-plane is a strong clustering near 90° for α and λ, which is indicative of upright porphyroblasts with S_i orientation close to S_e, implying little rotation. This can also be deduced from secondary clustering of small λ values with $\alpha = 0–30°$.

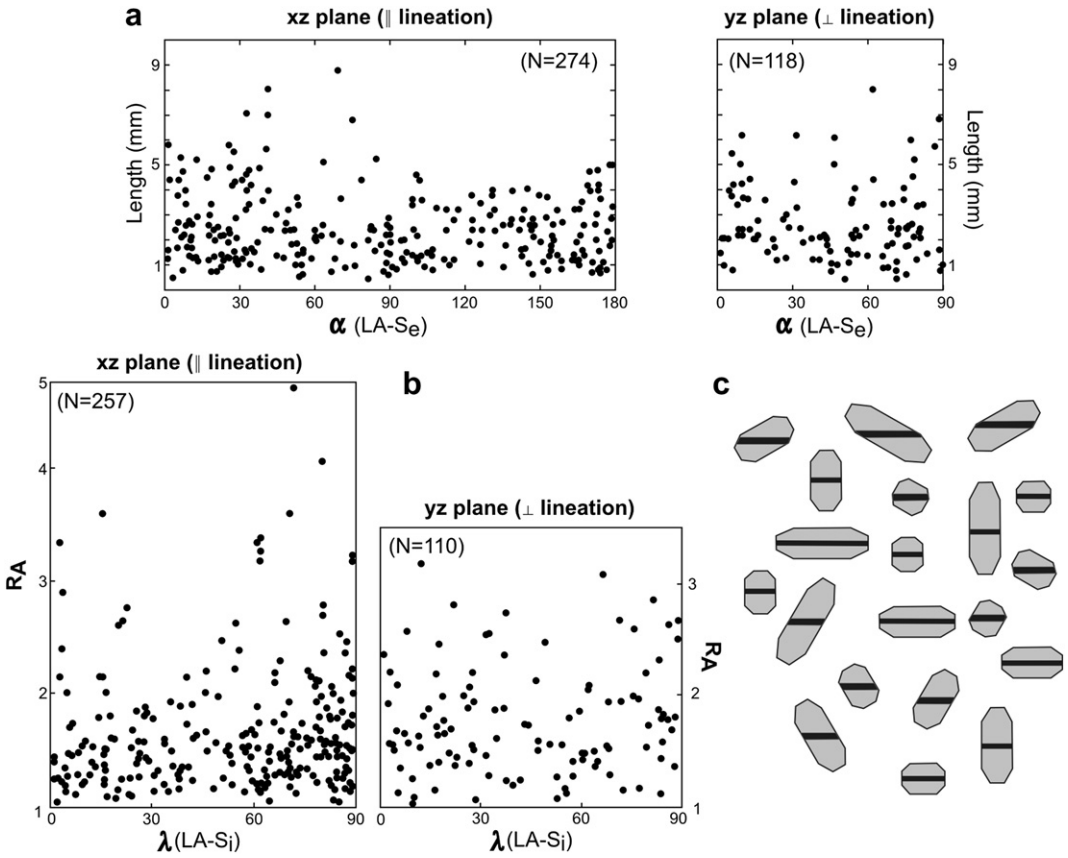

Fig. 6. No correlation exists between (a) porphyroblast length and obliquity of porphyroblast long axis to S_e (α) and (b) aspect ratio (R_A) and angle between long axis and S_i (λ). This can be interpreted as evidence for interkinematic random growth of staurolite porphyroblasts (c).

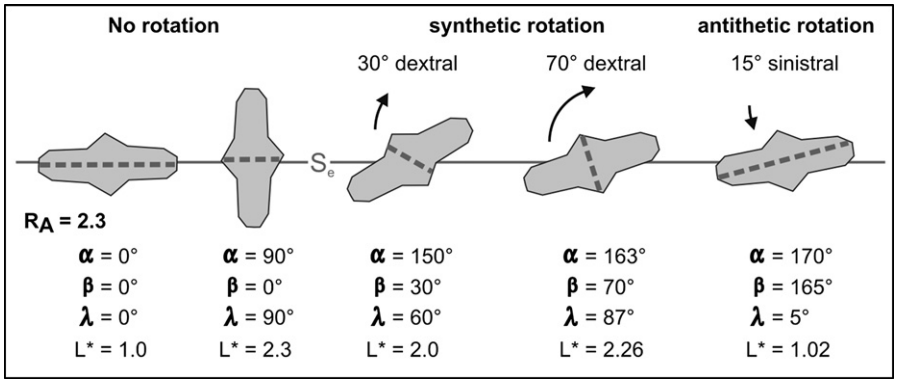

Fig. 7. Representative orientations of staurolite porphyroblasts in the xz-plane, parallel to mineral lineation. Blasts with an aspect ratio $R_A = 2.3$ that have not rotated, rotated in the shear direction (synthetic) and back rotated (antithetically) are shown with their appropriate values of α, β, λ and L^* associated with the inclusion trails, outlined by dashed grey line. Note, that rotations by multiples of 180°, or in the case of antithetic rotation shown here, a synthetic rotation by 165° would produce the same results. However, additional evidence, e.g. spiral-shaped S_i–S_e trails or decoupling between blast and matrix, should confirm stronger rotation.

L^* denotes the ratio between the length of the porphyroblast long axis and the length of S_i passing through the centre of the best-fit ellipse. It reflects the pre-kinematic orientation of a porphyroblast. L^* can attain a maximum value that equals R_A when S_i lies orthogonal to the long axis, i.e. $\lambda = 90°$, indicating that the crystal long axis grew in a direction perpendicular to the plane of schistosity. Large L^* values represent porphyroblasts with highly elongated shapes and S_i strongly oblique to their long axes. The minimum value for L^* is 1.0 and reflects parallelism between S_i and porphyroblast long axis. High-L^* blasts in the xz-plane with $\alpha = 180°$ and $\beta = 90°$ represent elongated grains lying subparallel to the schistosity with S_i strongly oblique to their long axis (Fig. 8b). A positive correlation between L^* and α can be observed for high-R_A blasts (>2). A different pattern is seen in the yz-plane, where β values rarely exceed 45° (Fig. 5a). In that section, high-L^* blasts tend to possess relative small β values, indicative of nearly orthogonal orientation of their long axes with respect to the schistosity, while S_i lies at low angles to S_e. In the yz-plane elongated blasts have retained a position, either parallel or orthogonal to the external schistosity, while their S_i displays small oblique angles with S_e.

In the plane parallel to schistosity (xy), the angle δ between staurolite long axis and stretching lineation bears no correlation with the orientation of S_i to the lineation (ϵ). The intersection lineation of the internal foliation lies nearly orthogonal to the shear direction (Fig. 8c). The angle λ between S_i and the long axis, on the other hand, shows a good correlation with δ. Small λ values are observed in blasts which lie nearly orthogonal to the stretching lineation ($\delta \sim 90°$), while increasingly larger λ is recorded in staurolite crystals whose long axes are more oblique to the lineation ($\delta \neq 90°$). Long axes parallel to the mineral lineation show maximum λ values.

The ellipticity of a blast and the relative length of its internal foliation can best be described by the relation between R_A and L^*, the ratio between the lengths of S_i and the short axis SA of the best-fit ellipse: LS_i/SA (Fig. 9). A minimum value of 1 indicates that S_i is oriented parallel to the short axis (Fig. 9a). Maximum values are realized by blasts with the highest aspect ratios, 5.1 for samples of this study in the xz-direction, indicating parallelism of S_i with long axis of the blast. The λ values which can be expected for given R_A and L^* are derived from the equation describing an ellipse in a Cartesian coordinate system (see Appendix, Fig. A1). The observed staurolite porphyroblasts record angular relationships predicted by the theoretical model (Fig. 9b). Long axes oriented subparallel to internal foliations (small λ) are recorded in blasts with large R_A/L^* values. Since R_A/L^* depends on the initial aspect ratio, also objects with small R_A/L^* can have small λ values. However, λ values over 60° can only be attained by low-R_A/L^* clasts, where S_i is nearly orthogonal to the long axis. When compared with the angle β between S_i and S_e, R_A/L^* displays a negative correlation (Fig. 9c). High-R_A/L^* blasts have small β angles, their elongated shapes with S_i paralleling their long axes are aligned to the schistosity. Staurolite porphyroblasts whose S_i lie orthogonal to the long axis (low-R_A/L^*) have the largest β values, they have rotated up to 90° or more.

6. Discussion

6.1. Interkinematic staurolite porphyroblast growth

Staurolite porphyroblasts in a fine-grained mica–quartz schist with a well-developed schistosity record peak M_1 regional metamorphism (Mezger and Passchier, 2003). Straight and parallel inclusion trails in staurolite, representing overgrown grains of the quartz-rich layers or microlithons of the main schistosity, are indicative of crystallization during a period of little deformation. Unconstricted growth is inferred from apparent lack of correlation between a) absolute porphyroblast length and long axes orientation relative to S_e, and b) obliquity of inclusion trails with long axes and aspect ratios in sections parallel and perpendicular to mineral lineation (Fig. 6a, b). While staurolite crystals grew at random, incorporated inclusion trails are oriented parallel (Fig. 6c).

6.2. Porphyroblast rotation

The ESE-directed shearing (D_{2a}) in the southern Bossòst dome reactivated the existing schistosity, as continuation of S_i into S_e in some staurolite blasts indicates. The geometry of shape orientations and the obliquity of inclusion trails with S_e differ significantly between three orthogonal planes. Intersection lineations of S_i with the planes perpendicular to foliation and lineation (yz) and parallel to foliation (xy) approximately lie at small angles around the y-direction. In contrast, in the xz-plane, S_i obliquity to $S_{1/2}$ varies significantly (Figs. 5 and 10). These observations concur with rotation of staurolite porphyroblasts with respect to the main schistosity around axes roughly aligned to the y-direction, orthogonal to the stretching lineation.

Rotation of porphyroblasts in the xz-plane depends primarily on three factors: the aspect ratio of a porphyroblast, the initial orientation of its long axis, and the relation between pure and simple shear (Ghosh and Ramberg, 1976). Interferences by neighbouring blasts causing local flow partitioning have to be considered as well (Tikoff and Teyssier, 1994). Despite the limitations of 2D-sections, several important observations can be made in the staurolite schist from the Bossòst dome. The sense of rotation is uniform, synthetic

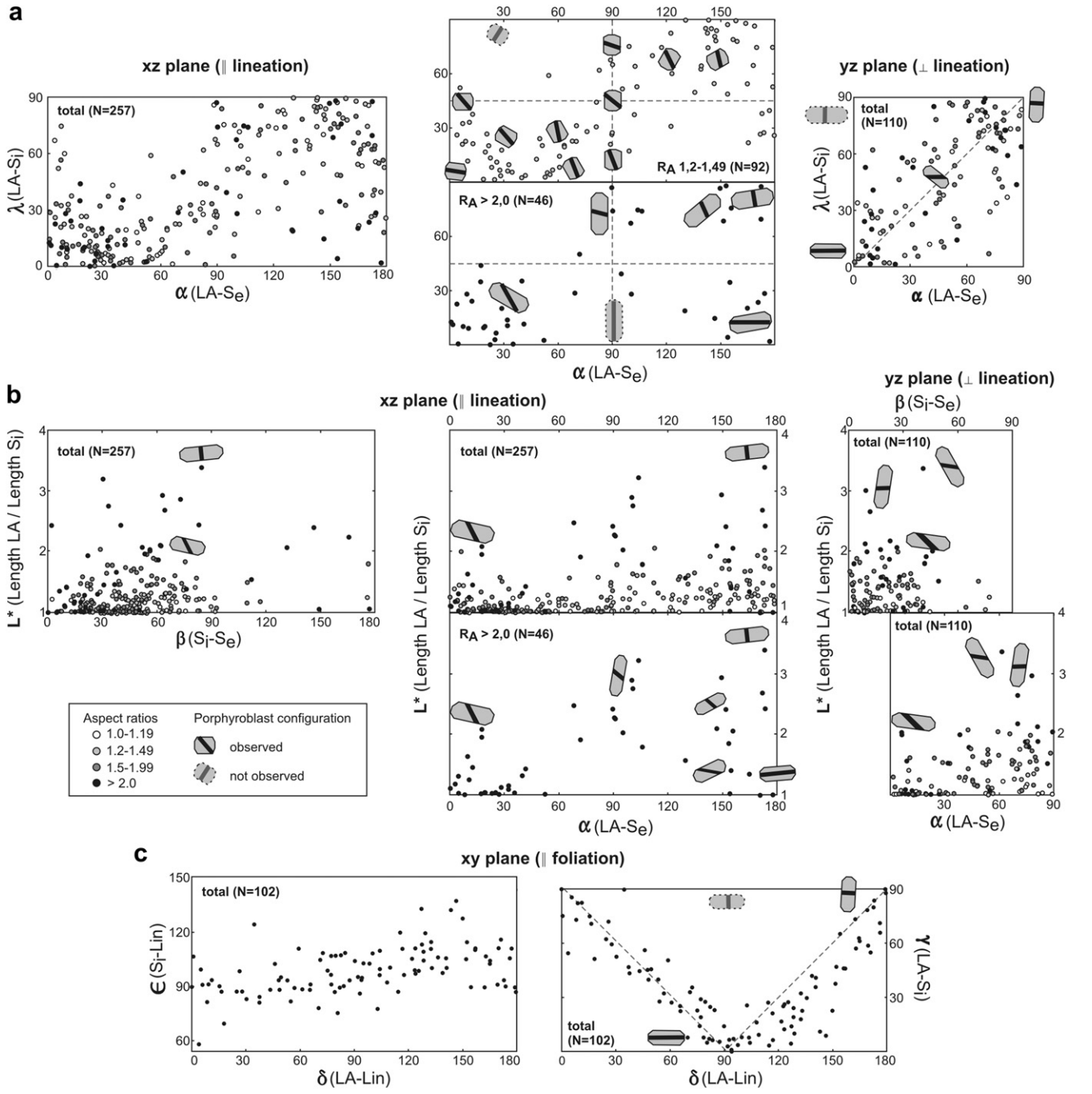

Fig. 8. Angular relationships between α, β, λ, L^* in the xz- and yz-planes, and S_i and long axes with lineation direction in the xy-plane. Sketches of porphyroblasts exemplify selected conditions and aspect ratios. Significant differences between xz- and yz-planes can be observed. Staurolite porphyroblasts are divided into four groups of aspect ratios. (a) α/λ plot shows S-shaped data distribution in the xz-plane. Small-R_A (1.2–1.49) blasts are represented across continuous values, while larger R_A-blasts preferably lie with their long axes at small angles (<30°) to S_e, with small α, λ or large α, λ. In the yz-plane, α is correlated positively with λ, in such a way that S_i broadly parallels S_e. (b) L^*/α and L^*/β plots of xz-planes show porphyroblasts with high L^* values, i.e. elongated blasts with high LA-S_i angles (λ), preferentially lie with their long axes parallel to and S_i orthogonal to the schistosity. In the yz-plane, long axes of blasts with large L^* values (>2) are strongly oblique to S_e, while S_i lies at small angles S_e. (c) In sections parallel to the schistosity, the angle ϵ between S_i and the mineral lineation is nearly orthogonal and not correlated with orientation of long axes. In contrast, λ is correlated with the angle δ between long axis and mineral lineation. Orthogonal δ values correspond with small λ angles, i.e. blasts with S_i parallel to long axes are oriented perpendicular to the stretching lineation. λ increases with decreasing obliquity to the mineral lineation. Long axes parallel to the mineral lineation show maximum λ values, i.e. the orientation of the long axes may change, but not the angle between S_i and the shear direction.

with respect to the shear direction, in each section. The relation between initial long axis orientation and aspect ratio is best expressed by the R_A/L^* ratio, the ratio between length of inclusion trails and the short axis, as explained in Section 5.3 (Fig. 9c). The table in Fig. 10c shows a strong negative correlation between R_A/L^* and the angle of rotation in the xz-plane. Large L^* values imply equally large λ, i.e. S_i lies orthogonal to long axis, and the R_A/L^* value is close to 1, enabling maximum rotation (see blast 1 in Fig. 10c). With increasing R_A/L^* the absolute aspect ratios become larger and L^* smaller, i.e. S_i lies parallel to the long axes. Such blasts tend not to rotate (#7 and 8 in Fig. 10c, Fig. 2b). In general, it can be stated that with increasing R_A/L^* porphyroblasts are more elliptical, are

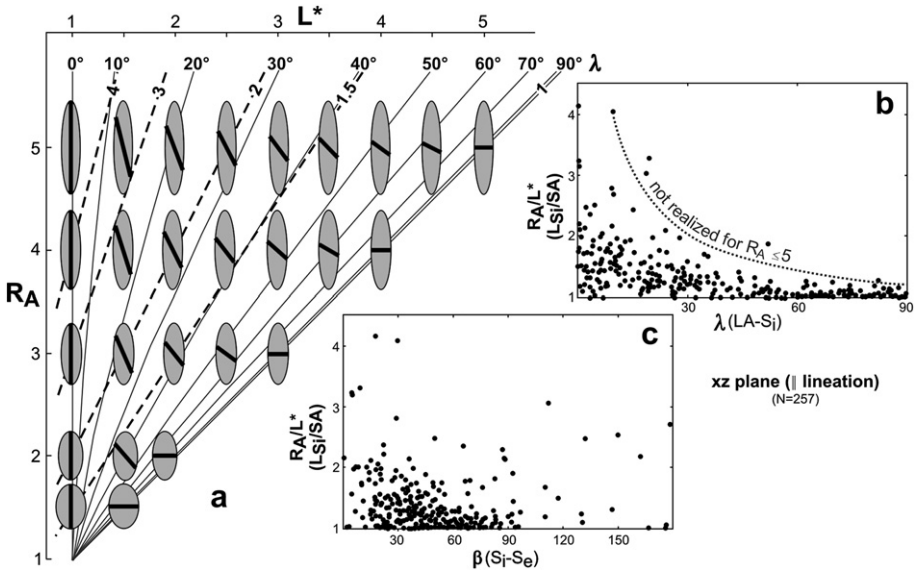

Fig. 9. (a) Diagram outlines the relation between ellipticity R_A of a blast, the ratio R_A/L^* between lengths of S_i and short axis SA, and the angle λ between long axis and S_i. Schematic porphyroblasts with representative inclusion trails are shown for clarification. Isopleths of λ are outlined in grey lines and determined by equation (3). Isopleths representing R_A/L^*, depending on the original aspect ratios, are shown as dashed black lines. Only large aspect ratios can produce large R_A/L^* values. Small λ values correlate with the largest R_A/L^* possible for the existing aspect ratios. λ increases with decreasing R_A/L^* values, so that $R_A/L^* = 1$ implies orthogonal orientation of S_i with respect to the long axis. (b) Microstructural observations correspond well with the predicted values. Most of the staurolite porphyroblasts lie within the limits of possible orientations, indicated by the dotted grey line. Large λ is recorded only in low-R_A/L^* grains, while large R_A/L^* values correlate with small λ. Since aspect ratios in the xz-plane do not exceed 5.1, high-R_A/L^* staurolite possesses small λ values. (c) R_A/L^* correlates negatively with β. High-R_A/L^* grains have S_i lying close to parallel with the external foliation, while blasts with S_i nearly orthogonal to S_e have small R_A/L^* values, i.e. S_i is perpendicular to the long axis.

initially aligned parallel to the flow plane ($\alpha \sim 0$), and have rotated only by small amounts during subsequent shearing ($\beta \sim 0$). In contrast, maximum rotation of 90° can be observed in blasts with low R_A/L^*, but high R_A and L^*.

6.3. Estimation of shear strain and vorticity during D_{2a}

In simple shear flow equant rigid particles undergo rotation that is equal to half the bulk shear strain (Jeffrey, 1922). The maximum synthetic rotation observed in the staurolite schist is 120°, which would imply a shear strain of $\gamma = 4.3$ in simple shear flow (Passchier and Trouw, 2005, p. 137). Several blasts with long axes initially oriented at small angles ($\alpha = 20$–30°) have subsequently rotated synthetically (Fig. 2a, #4 and 6 in Fig. 10c). Marques and Coelho (2003) calculated rotational behaviour of rigid objects during transpressional deformation with different proportions of pure and simple shear rates ($S_r = \dot{\varepsilon}/\gamma'$). With a significant pure shear component ($S_r = 1$) objects with $R_A = 3$ oriented at angles (α) less than 60° will back rotate. Assuming smaller pure shear influence ($S_r = 0.1$ and 0.25) objects with their long axis inclined at 20° and 30° (Fig. 2a, # 4 and 6 in Fig. 10c) will rotate synthetically. The observed finite rotations of these blasts by 20° and 40° correspond to a shear strain $\gamma = 2$–4 (Fig. 3, Marques and Coelho, 2003). In the sample studied here, simple shear ($W_k \geq 0.8$–0.9) was the dominating flow type, and pure shear contributed, if at all, only in a modest way. Calculations by Sara Coelho show that at shear strain $\gamma = 4$ and vorticity $W_k = 0.89$ objects with $R_A = 3$ are expected to rotate up to 120° when they will attain a stable position (Fig. B.5.2. in Passchier and Trouw, 2005). Higher finite strain would have rotated all porphyroblasts into stable positions, which is not observed in this rock.

6.4. Post-shearing crenulation rotation

Submillimeter-scale crenulation folds observed in the yz-plane are microscopic evidence of D_3 deformation, which is also responsible for southerly verging meso- and macroscale folds throughout the Bossòst dome. Though crenulation fold axes lie approximately parallel to mineral lineation, a post-intrusive age is corroborated by folded granitic sills (Fig. 11 in Mezger and Passchier, 2003). Horizontal shortening orthogonal to the D_{2a} flow direction is likely the reason for the rotation of S_i out of the *y*-direction, which happened when elongated blasts initially at high angle (50–80°) to schistosity rotated around the crenulation fold axis into the vertical (left blast in Fig. 2c, #10 and 12 in Fig. 10c). The concentration of high-R_A blasts long axes oriented orthogonal to S_e and coexisting clockwise and counterclockwise rotation of S_i confirms this idea (Figs. 2c and 5a). The effects of rotation around the crenulation axis parallel to the *x*-direction are far less significant. For example, rotation of an originally 45°-dipping (β) plane by 40° around the crenulation axis results in an apparent dip of 54° in the direction of the rotation axis. Planes with other initial dip angles deviate less than 9°. Since most D_3 rotations amount to less than 30°, the effects on the S_i obliquity can be regarded as rather small.

6.5. Evidence against porphyroblast non-rotation

A key argument of opponents of porphyroblast rotation is the decoupling between blast and the matrix. Progressive strain partitioning results in the development of anastomosing high strain shear zones around strong porphyroblasts forming ellipsoidal low strain islands (Fay et al., 2008; Bell, 1985). Further grow of porphyroblasts into high strain zones dominated by simple shear flow is thought to be impossible. Porphyroblasts are locked in a zone of coaxial deformation and are prevented from rotation. These models commonly involve an earlier foliation strongly oblique to the shear plane and subsequent development of a crenulation cleavage around rigid porphyroblasts (Bell and Bruce, 2007).

However, significant strain partitioning does not occur in all rocks. The flow plane in the Bossòst staurolite schist lies parallel to the previously existing schistosity, so that D_{2a} shearing did not

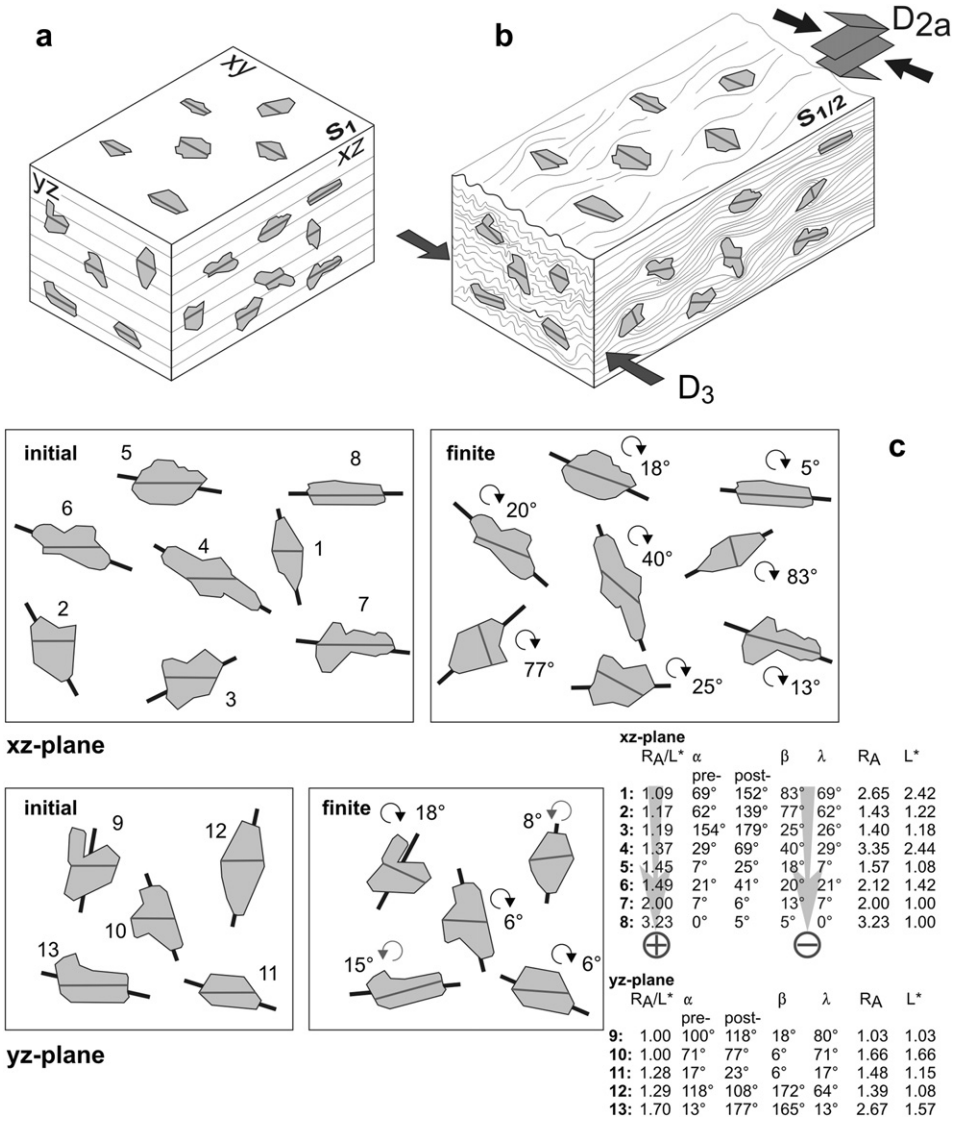

xz-plane

	R_A/L^*	α pre-	α post-	β	λ	R_A	L^*
1:	1.09	69°	152°	83°	69°	2.65	2.42
2:	1.17	62°	139°	77°	62°	1.43	1.22
3:	1.19	154°	179°	25°	26°	1.40	1.18
4:	1.37	29°	69°	40°	29°	3.35	2.44
5:	1.45	7°	25°	18°	7°	1.57	1.08
6:	1.49	21°	41°	20°	21°	2.12	1.42
7:	2.00	7°	6°	13°	7°	2.00	1.00
8:	3.23	0°	5°	5°	0°	3.23	1.00

yz-plane

	R_A/L^*	α pre-	α post-	β	λ	R_A	L^*
9:	1.00	100°	118°	18°	80°	1.03	1.03
10:	1.00	71°	77°	6°	71°	1.66	1.66
11:	1.28	17°	23°	6°	17°	1.48	1.15
12:	1.29	118°	108°	172°	64°	1.39	1.08
13:	1.70	13°	177°	165°	13°	2.67	1.57

Fig. 10. Block diagram showing representative staurolite porphyroblast orientation observed in the Arres staurolite–mica schists. (a) Schist after D_1 event, which resulted in development of S_1 foliation and regional metamorphism with randomly oriented staurolite porphyroblast growth. (b) Present day appearance of schist after D_{2a} non-coaxial deformation and D_3 shortening. (c) Views of xz- and yz-planes with initial, post-D_1, pre-D_{2a}, and finite, post-D_{2a}, -D_3 porphyroblast orientation. Black lines underlying porphyroblasts outline long axes of best-fit ellipses obtained from ImageJ. Initial orientations are inferred from the assumption that S_i was initially aligned horizontally. Porphyroblasts of the initial yz-plane are scaled in the *z*-direction compared to the finite plane, to account for sectioning effects due to rotation in the *y*-direction. The finite sections show representative porphyroblasts with various parameter relationships, listed in the tables. Porphyroblasts are ranked according to R_A/L^* values. See text for discussion.

create a new foliation. The competence contrast between mica-rich layers and mica-bearing quartz-rich zones is not sufficient to initiate strain partitioning, and the whole schist deformed rather homogeneously. Furthermore, staurolite porphyroblasts nucleated before the onset of shearing and overgrew mica- and quartz-rich layers, whose spacing is narrower than the average size of staurolite blasts. Thus, staurolite porphyroblasts were locked in the deforming matrix and high strain zones, aside from some minor strain caps within the mica layers, did not develop around the porphyroblasts. No significant decoupling between porphyroblasts and matrix has occurred, which is also evident from continuation of external foliation with inclusion trails.

Another model proposing porphyroblast non-rotation involves rotation of the foliation while porphyroblasts remain a stable orientation. An important indication for foliation rotation is parallelism of inclined inclusion trails in all contemporaneous porphyroblasts (Aerden, 1995). However, foliation rotation cannot satisfactorily explain the variable orientation of inclusion trails in the staurolite porphyroblasts, so that it can be excluded as a major process in the formation of the Bossòst staurolite schist fabric.

7. Conclusions

1. Idioblastic staurolite porphyroblasts can serve as valuable kinematic indicators for deformation events that postdate regional metamorphism, because they commonly form relative large prophyroblasts with abundant inclusion trails preserving previous fabrics. However, later contact metamorphism may lead to partial or complete consumption and loss of euhedral shape.
2. The sense and amount of rotation of staurolite porphyroblasts depend on growth orientation and their aspect ratio, as well as the type of shear flow and the magnitude of shear. Staurolite from the Bossòst dome shear zone has rotated synthetically in the shear direction, even when their long axes are initially antithetically inclined at low angles to the shear plane. This corresponds to dominant simple shear flow. The maximum

rotation is observed in blasts with S_i oriented orthogonal to the mineral long axis. Blasts with S_i parallel to their long axes have not rotated significantly, suggesting that they maintained an initial stable position. The fact that not all elongated blasts have rotated into parallelism with the shear plane indicates that these rocks were deformed with a maximum shear strain $\gamma = 4–5$.

3. Deformation of the matrix is homogeneous enough to prevent significant strain partitioning that would enhance decoupling between matrix and porphyroblast. The main arguments for porphyroblast non-rotation, strain partitioning between anastomosing high-strain shear and low strain coaxial ellipsoidal zones, cannot be applied to the Bossòst staurolite schist.
4. Staurolite commonly forms irregular interpenetrating growth twins with various aspect ratios, representing rigid objects with different rotational behaviours. Thus, staurolite porphyroblasts may serve as sensitive vorticity and shear strain gauges, as it is already applied for other minerals (e.g. biotite, Holcombe and Little, 2001).

Acknowledgements

Interest in the statistical analyses of staurolite orientation data was raised by a comment from Neil Mancktelow following a talk at the ETH Zurich. Christian Born is thanked for providing equation (3) to construct the diagram of Fig. 9a. Critical reviews by Rod Holcombe and Dazhi Jiang helped to significantly improve the manuscript.

Appendix

Approximation of the shape of a porphyroblast by an ellipse calculated by ImageJ further allows investigating the relations between λ, the angle between blast long axis and internal foliation, the length of the S_i, and the aspect ratio. The length of the inclusion trail is defined as the length of a line going through the centre of the ellipse (Fig. 3). Values for λ at given S_i lengths and R_A can be derived from the equation defining an ellipse in a Cartesian coordinate system (Fig. A1):

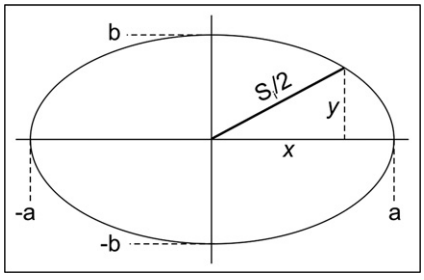

Fig. A1. Ellipse in Cartesian coordinate system used to derive length of S_i passing through the centre of the ellipse. See Appendix for discussion.

$$\frac{x^2}{a^2}+\frac{y^2}{b^2} = 1 \quad (1)$$

with $a = LA/2$ and $b = SA/2$ are the halves of the lengths of the long axis and short axes, respectively. x^2 and y^2 are the catheti, with $x^2 + y^2 = (S_i/2)^2$. The angle λ between $S_i/2$ and a is defined as

$$\lambda = \arctan\frac{x}{y} \quad (2)$$

Substitution of x and y leads to the following equation:

$$\lambda = \arctan\sqrt{\frac{LA^2 - S_i^2}{R_A^2 S_i^2 - LA^2}} \quad (3)$$

References

Aerden, D.G.A.M., 1995. Porphyroblast non-rotation during crustal extension in the Variscan Lys-Caillaouas Massif, Pyrenees. Journal of Structural Geology 17, 709–725.
Arbaret, L., Mancktelow, N.S., Burg, J.P., 2001. Effect of shape and orientation on rigid particle rotation and matrix deformation in simple shear flow. Journal of Structural Geology 23, 113–125.
Bell, T.H., 1985. Deformation partitioning and porphyroblast rotation in metamorphic rocks: a radical reinterpretation. Journal of Metamorphic Geology 3, 109–118.
Bell, T.H., Bruce, M.D., 2007. Progressive deformation partitioning and deformation history: evidence from millipede structures. Journal of Structural Geology 29, 18–35.
Biermeier, C., Stüwe, K., 2003. Strain rates from snowball garnets. Journal of Metamorphic Geology 21, 253–268.
Bons, P.D., Jessell, M.W., Griera, A., Fay, C., Bell, T.H., Hobbs, B.E., 2009. Porphyroblast rotation versus nonrotation: conflict resolution!: comment and reply. Geology 37, e182–e188.
Busa, M.D., Gray, N.H., 1992. Rotated staurolite porphyroblasts in the Littleton schist at Bolton, Connecticut, USA. Journal of Metamorphic Geology 10, 627–636.
Fay, C., Bell, T.H., Hobbs, B.E., 2008. Porphyroblast rotation versus nonrotation: conflict resolution! Geology 36, 307–310.
Ghosh, S.K., Ramberg, H., 1976. Reorientation of inclusions by combination of pure shear and simple shear. Tectonophysics 34, 1–70.
ten Grotenhuis, S., Passchier, C.W., Bons, P.D., 2002. The influence of strain localisation on the rotation behaviour of rigid objects in experimental shear zones. Journal of Structural Geology 24, 485–499.
Holcombe, R.J., Little, T.M., 2001. A sensitive vorticity gauge using rotated porphyroblasts, and its application to rocks adjacent to the Alpine Fault, New Zealand. Journal of Structural Geology 23, 979–989.
Jeffrey, G.B., 1922. The motion of ellipsoidal particles immersed in a viscous fluid. Proceedings of the Royal Society of London A 102, 161–179.
Johnson, S.E., 2009. Porphyroblast rotation and strain localization: debate settled! Geology 37, 663–666.
Johnson, S.E., Dupee, M.E., Guidotti, C.V., 2006. Porphyroblast rotation during crenulation cleavage development: an example from the aureole of the Moose-lookmeguntic pluton, Maine, USA. Journal of Metamorphic Geology 24, 55–73.
Johnson, S.E., Lenferink, J., Marsh, J.H., Price, N.A., Koons, P.O., West Jr., D.P., 2009. Kinematic voricity analysis and evolving strength of mylonitic shear zones: new data and numerical results. Geology 37, 1075–1078.
Lister, G.S., Forster, M., 2009. Porphyroblast rotation versus non-rotation: conflict resolution: comment. Geology 37, e201.
Mancktelow, N.S., Arbaret, L., Pennacchioni, G., 2002. Experimental observations on the effect of interface slip on rotation and stabilisation of rigid particles in simple shear and a comparison with natural mylonites. Journal of Structural Geology 24, 567–585.
Marques, F.O., Coelho, S., 2001. Rotation of rigid elliptical cylinders in viscous simple shear flow: analogue experiments. Journal of Structural Geology 23, 609–617.
Marques, F.O., Coelho, S., 2003. 2-D shape preferred orientations of rigid particles in transtensional viscous flow. Journal of Structural Geology 25, 841–854.
Mezger, J.E., 2010. Mimicking syntectonic growth: cordierite overgrowth of earlier rotated staurolite porphyroblasts, strain caps and deflected foliation. Journal of Structural Geology 32, 703–708.
Mezger, J.E., Chacko, T., Erdmer, P., 2001. Metamorphism along a late Mesozoic accretionary continental margin: a case study from the northern Coast Belt of the North American Cordillera. Journal of Metamorphic Geology 19, 121–138.
Mezger, J.E., Passchier, C.W., Régnier, J.-L., 2004. Metastable staurolite-cordierite assemblage of the Bossòst dome: late Variscan decompression and polyphase metamorphism in the Axial Zone of the central Pyrenees. Comptes Rendus Geoscience 336, 827–837.
Mezger, J.E., Passchier, C.W., 2003. Polymetamorphism and ductile deformation of staurolite-cordierite schist of the Bossòst dome: indication for Variscan extension in the Axial Zone of the central Pyrenees. Geological Magazine 140, 595–612.
Miyake, A., 1993. Rotation of biotite porphyroblasts in pelitic schist from the Nukata area, central Japan. Journal of Structural Geology 15, 1303–1313.
Passchier, C.W., 1987. Stable positions of rigid objects in non-coaxial flow—a study in vorticity analysis. Journal of the Geological Society, London 9, 679–690.
Passchier, C.W., Trouw, R.A.J., 2005. Microtectonics. Springer Verlag, Berlin, Heidelberg.
Ribbe, P.H., 1982. Staurolites. In: Ribbe, P.H. (Ed.), Orthosilicates. Reviews in Mineralogy, vol. 5. Mineralogical Society of America, pp. 171–188.
Robyr, M., Carlson, W.D., Passchier, C.W., Vonlanthen, P., 2009. Microstructural, chemical and textural records during growth of snowball garnet. Journal of Metamorphic Geology 27, 423–437.
Schoneveld, C., 1977. A study of some typical inclusion patterns in strongly paracrystalline-rotated garnets. Tectonophysics 39, 453–471.
de Sitter, L.U., Zwart, H.J., 1960. Geological map of the Central Pyrenees, Sheet 4 Valle de Aran, Spain. Geological Institute, University of Leiden, scale 1:50,000.
Tikoff, B., Teyssier, C., 1994. Strain and fabric analyses based on porphyroclast interaction. Journal of Structural Geology 16, 477–491.
Williams, P.F., Jiang, D., 1999. Rotating garnets. Journal of Metamorphic Geology 17, 367–378.
Zwart, H.J., 1962. On the determination of polymetamorphic mineral associations, and its application to the Bosost area (Central Pyrenees). Geologische Rundschau 52, 38–65.